Tailoring a specialty alloy for Additive Manufacturing: From powder production to parameter optimisation

Tailoring a speciality alloy for Additive Manufacturing: From powder production to parameter optimisation

Ultra-high temperature materials, such as niobium-base alloys, have been limited to simple geometric designs due to their high working temperatures and related production costs. Now, thanks to the development of commercially available Nb-base alloy powders, it is possible to additively manufacture complex-shaped, high-performance components from this material. To do so, it is important to understand the full workflow, from powder production and characterisation, to determining the optimal process parameters for these speciality materials. In this article, Taniobis GmbH and Alloyed Ltd detail the process of preparing, characterising, and processing two such alloy powders.

Ultra-high temperature refractory alloys have the potential to perform at temperatures exceeding ~1050°C – outperforming even the most advanced Ni- and Co-base superalloys – due to the ceiling imposed by the strengthening phase stability and their high melting point. Niobium-base alloys such as C-103 are of particular interest, due to their relatively low density and good thermal conductivity, as well as excellent temperature and time-dependent mechanical properties (Fig. 1) [1, 2, 3].

As a result, Niobium-base alloys are commonly used in propulsion systems within the space and defence industry [4]. Until recently, typical applications have been limited to products with simple geometries made from sheet and bar; for instance, expansion chamber skirts made from TIG welded sheet. This is because ingot production is expensive and these alloys are challenging to fabricate into complex shapes due to their high hot working temperature. Because of the high cost of manufacture, C-103 is, by comparison, the most readily manufacturable, if not the strongest, Nb alloy on the market today.

Near-net shape manufacture of these alloys was previously not possible, as investment casting presents challenges around mould reactions and insufficient superheating, as well as being cost prohibitve for economic reasons such as loss of the alloy in gates [5]. Processing these unique high-temperature alloys in powder form allows for their near-net shape

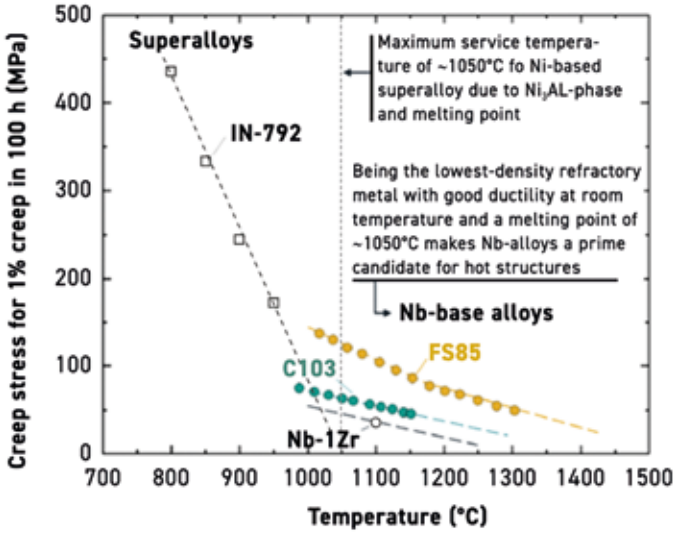

Fig. 1 Creep performance of various high-temperature alloys showing the superiority of Nb alloys. Data for superalloys extracted from [3]

		(wt.%)						(ppm)			
Alloy	**Analysis**	**Nb**	**Ta**	**Hf**	**W**	**Ti**	**Zr**	**C**	**H**	**N**	**O**
C-103	Chemical	88.7	0.2	9.6	< 0.1	1.0	0.2	29	< 10	44	198
	EDX area	89.2	--	9.7	--	0.1	1.0	0 (1)	--	--	0 (1)
	EDX spot 1	90.5	--	8.5	--	0.0	1.1	0 (1)	--	--	0 (1)
	EDX spot 2	79.2	--	19.6	--	0.1	--	0 (1)	--	--	0 (1)
FS-85	Chemical	60.8	28.3	0.03	10.0	0.01	1.0	< 10	< 10	19	289
	EDX area	61.7	26.3	--	9.8	--	2.3	0 (1)	--	--	0 (1)
	EDX spot 1	68.2	21.1	--	5.8	--	4.9	0 (1)	--	--	0 (1)
	EDX spot 2	58.3	29.3	--	10.4	--	1.9	0 (1)	--	--	0 (1)
(1) below detection limit | -- not determined											

Table 1 The chemical composition of C-103 and FS-85 powders determined spectroscopically (ICP-OES) and by carrier gas hot extraction/combustion analysis

manufacture using Laser Beam Powder Bed Fusion (PBF-LB), Electron Beam Powder Bed Fusion (PBF-EB), Directed Energy Deposition (DED), and other advanced forms of Powder Metallurgy. These technologies have major advantages over conventional processing, including cheaper part production thanks to their more efficient use of material and the ability to produce geometrically complex components with minimal waste or post-processing.

The ability to manufacture complex shapes from C-103 [6] and FS-85 (here described for the first time) via PBF-LB enables new applications such as structures for high-velocity flight and re-entry guidance, and enables the production of higher temperature gas turbines for power generation and jet propulsion. This article will describe in detail the preparation of Nb alloy powders for application in advanced metal powder-based manufacturing technologies.

Alloy powder preparation

Nb-base C-103 and FS-85 alloy powders developed at Taniobis GmbH, Germany, are commercially available in the form of AMtrinsic® C-103 or AMtrinsic® FS-85 pre-alloyed powders [7]. Due to the lack of suitable crucible materials for conventional gas atomisation, they are atomised by Electrode Induction-Melting Gas Atomisation (EIGA) [8] of pre-alloyed electrodes. In this study, the electrodes were electron beam melted with dimensions of ca. dxl = 45 x 650 mm. Prior to their use, a 90° tip was machined to fit the shape and dimension of the induction coil. The pre-alloyed rods were atomised in a purified Ar (4.6, Linde) atmosphere through a Laval nozzle and the as-obtained raw powders sieved to remove the fine powder fraction (< 10 µm). Finally, the sieved powders were classified through 63 µm, 105 µm and 150 µm meshes. This classification provided powders with particle size distributions typically applied in PBF-LB (10–63 µm), PBF-EB (63–105 µm) or DED (105–150 µm).

"The ability to manufacture complex shapes from C-103 and FS-85 via PBF-LB enables new applications such as structures for high-velocity flight and re-entry guidance, and enables the production of higher temperature gas turbines for power generation and jet propulsion."

Alloy powder characterisation

C-103 and FS-85 PBF-LB alloy powders were fully chemically characterised by a combination of ICP-OES and carrier gas hot extraction and/or combustion analysis, as well as morphologically by X-ray diffraction (XRD) and Scanning Electron Microscopy (SEM)/Energy Dispersive X-Ray Analysis (EDX). Their flowability was investigated using Hall Flow measurements.

The chemical compositions of the C-103 and FS-85 powders,

determined spectroscopically (ICP-OES) and by carrier gas hot extraction/combustion analysis, are provided in Table 1. For comparison, the overall composition and the composition of selected spots determined by EDX are given. The chemical compositions of the atomised powders correspond well with those of conventionally processed materials. However, due to the much higher surface areas, the contents of the light elements (i.e., C, N and O) are slightly higher than in the cast solids. Investigations by XRD, shown in Fig. 2, point to the fact that C-103 and FS-85 alloy powders crystallised in the body-centred cubic crystal structure. A comparison with pure Nb shows very similar appearance of the XRD patterns with the typical 110, 200 and 211 beta-phase reflections. Accordingly, C-103 and FS-85 can be considered as single-phase materials.

For application in powder bed Additive Manufacturing processes, good powder processability is mandatory [9]. A spherical particle shape is one important requirement to guarantee free flow and ensure a homogeneous distribution of the powder in each individual coating step. Other prerequisites are the absence of satellites, i.e. attachment of smaller particles on the surface of larger particles or agglomerates. The absence of pores or voids in the powders is necessary to avoid the inclusion of porosity in the built part. Both C-103 and FS-85 PBF-LB powders show an ideally spherical particle shape, as can be seen from the SEM images in Fig. 3. They have smooth surfaces and are fully deagglomerated. In addition, satellites are absent and, consequently, the powders possess very good flow properties. Their Hall Flow, according to ASTM B213, is 12 s (C-103) and 8 s (FS-85). Particle size measurements by means of laser diffraction indicate narrow distributions with d50 values of 34 µm and 39 µm. Tap densities are in the range of 5.5 g/cm³ (C-103)

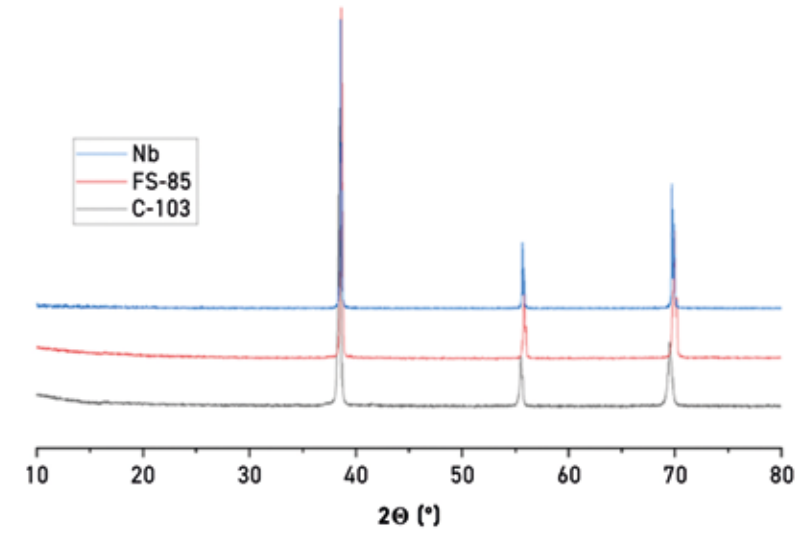

Fig. 2 XRD pattern of C-103 and FS-85 alloy powders and comparison with pure Nb powder

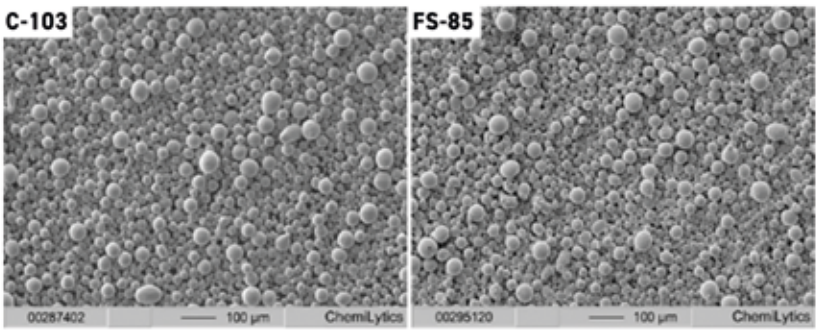

Fig. 3 SEM images of C-103 and FS-85 alloy powders recorded at 100x magnification

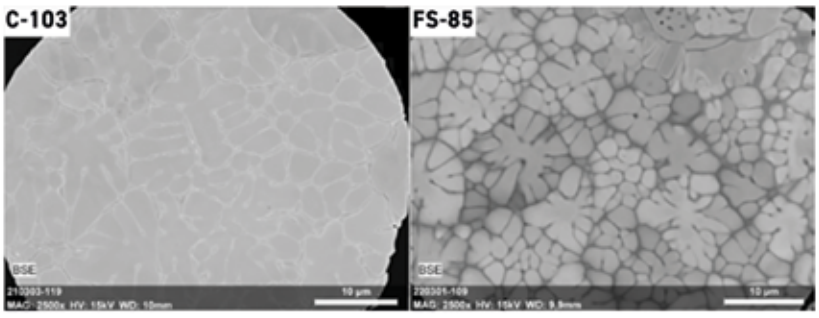

Fig. 4 BSE images of polished cross sections of C-103 and FS-85 alloy powders recorded at 2500x magnification

and 6.5 g/cm³ (FS-85). The higher density of FS-85 is attributed to its substantial Ta and W contents.

From the polished cross-sections shown in Fig. 4, it can be concluded that the particles are fully dense. Voids, defects or inhomogeneities are not observed. Interestingly, the BSE images of both C-103 and FS-85 show structural features with a more or less pronounced dendritic appearance. Similar observations have been made for Nb and Ta-modified Ti base alloys [10]. In C-103, they do not appear clearly, while the BSE image from FS-85 undoubtedly shows flower-like dendritic features. In addition,

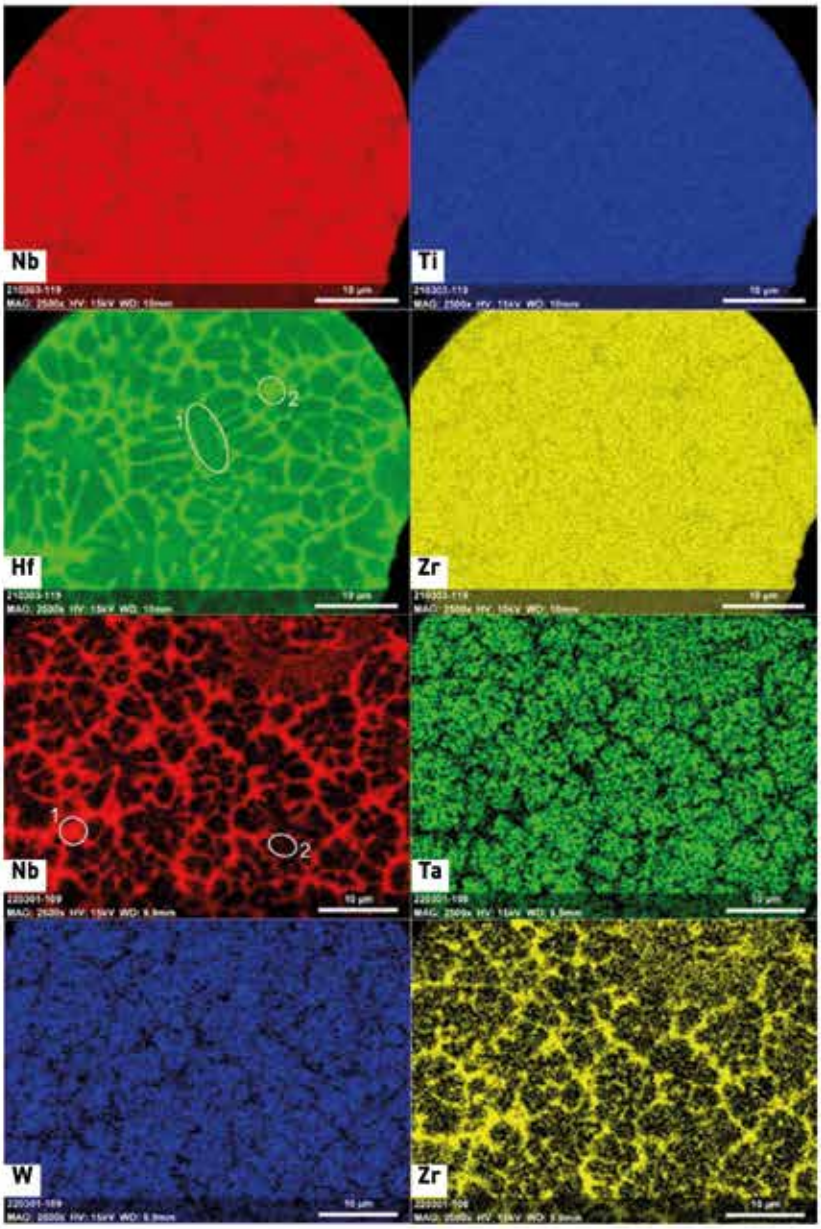

Fig. 5 EDX images of polished cross sections of C-103 (top) and FS-85 (bottom) alloy powders recorded at 2500 x magnification. The chemical composition of the entire area and selected spots 1 and 2 are provided in Table 1

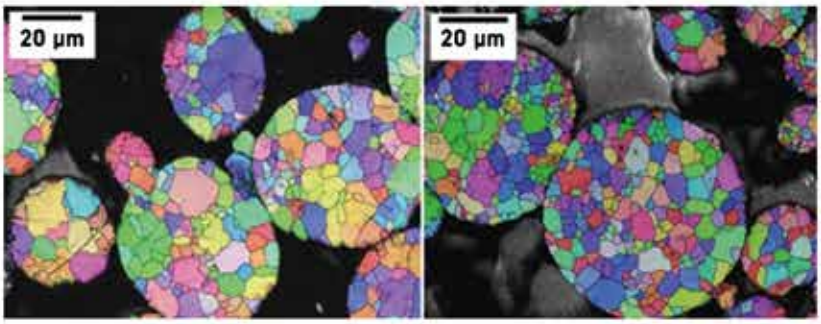

Fig. 6 EBSD of C-103 (left) and FS-85 (right) powders showing the grain structure within the powder particles

the contrast in the image of FS-85 is significantly higher than that of C-103.

The EDX images of C-103 and FS-85 powder provided in Fig. 5 show clear differences in the distribution of the elements. In C-103, chemical variation of the main components Nb and Hf is observed. Nb appears enriched in the dendritic phase while Hf is enriched in the inter-dendritic phase. This is clearly expressed by the different chemical compositions, which are highlighted in Table 1 of spots 1 and 2 in the Hf map of C-103. While the dendrite-type features contain 90.5 wt.% Nb and 8.5 wt.% Hf, the volumes between the dendrites consist of 79.2 wt.% Nb and 19.6 wt.% Hf. The secondary components Ti and Zr appear homogeneously distributed throughout the particle.

The element distribution in FS-85 is very different. None of the elements appear to be homogeneously distributed throughout the particles. There is a clear separation into Nb/Zr and Ta/W enriched volumes. In contrast to C-103, Nb appears with higher concentration in the inter-dendritic phase associated with Zr, whereas Ta and W occur preferentially in the dendrite phase. The chemical fluctuations of the elements in both phases are significantly more pronounced than with C-103. While spot 1 – which indicates the composition of the inter-dendrite phase – consists of 68.2 wt.% Nb, 21.1 wt.% Ta, 5.8 wt.% W and 4.9 wt.% Zr, the values in the dendritic structures (cf. spot 2) are 58.3 wt.%, 29.3 wt.%, 10.4 wt.% and 1.9 wt.%, respectively.

C-103 and FS-85 powder particles were also investigated by means of Electron Backscatter Diffraction (EBSD) to generate information on crystal size, structure and orientation. The average grain size of C-103 particles, at approx 20 µm, appears to be slightly coarser than in FS-85. This might be a consequence of the higher number of constituents in FS-85 than in C-103 and, conse-

quently, a higher entropy of the FS-85 system, exhibiting extensive crystallisation. Such an effect is well known for refractory metal high-entropy alloys.

Alloyed's process for AM parameter development

The additive manufacturability of C-103 and FS-85 was assessed by PBF-LB in a protective argon atmosphere using a Renishaw AM 400 pulsed fibre laser metal AM machine with a 1075 nm wavelength. Additively manufacturing any new alloy or composition requires single track experiments to be carried out at various AM machine settings to acquire information on melt pool thickness and depth. This is key to ensuring the melt pools overlap, creating sound builds without any remnant unfused powder. A single track also helps parameter selection by adjusting the trade-off between a stable scan track and keyhole formation due to high enthalpy. Fig. 7 provides a schematic of the various AM machine parameters tested. A snapshot of the single track samples is also shown; these were metallographically analysed to determine scan track stability and soundness. The scan track width and one-dimension energy density were plotted along with the ranking of the tracks based on the stability post metallographic analyses. This is shown in Fig. 8 and can be used as a map to visualise the effect of operating parameters on additive manufacturability.

The AMtrinsic C-103 and FS-85 powders, after being thoroughly characterised as described in the previous section, were additively manufactured with varied process parameters according to the design of experiment strategy. Cubes of dimension 10 x 10 x 10 mm were manufactured with varying processing parameters (shown in Table 2) at a fixed layer thickness of 30 µm. A meander laser scan path was applied with a rotation of 67° between consecutive layers.

Fig. 9 shows a snapshot of one particular DOE strategy of twelve cubes being additively manufactured. Once the optimised process parameter was narrowed down, a full test bar build was undertaken. After manufacturing the cubes, a full microstructural characterisation was performed to correlate the process parameters and microstructural attributes. The density of the cubes and the AM defects concentration (cracks and porosities measured through microstructural characterisation) were correlated with the build parameters such as laser power, exposure time, hatch and point distance.

The influence of the processing parameters such as laser power, scan speed, hatch, powder bed thickness, etc, on the quality of the

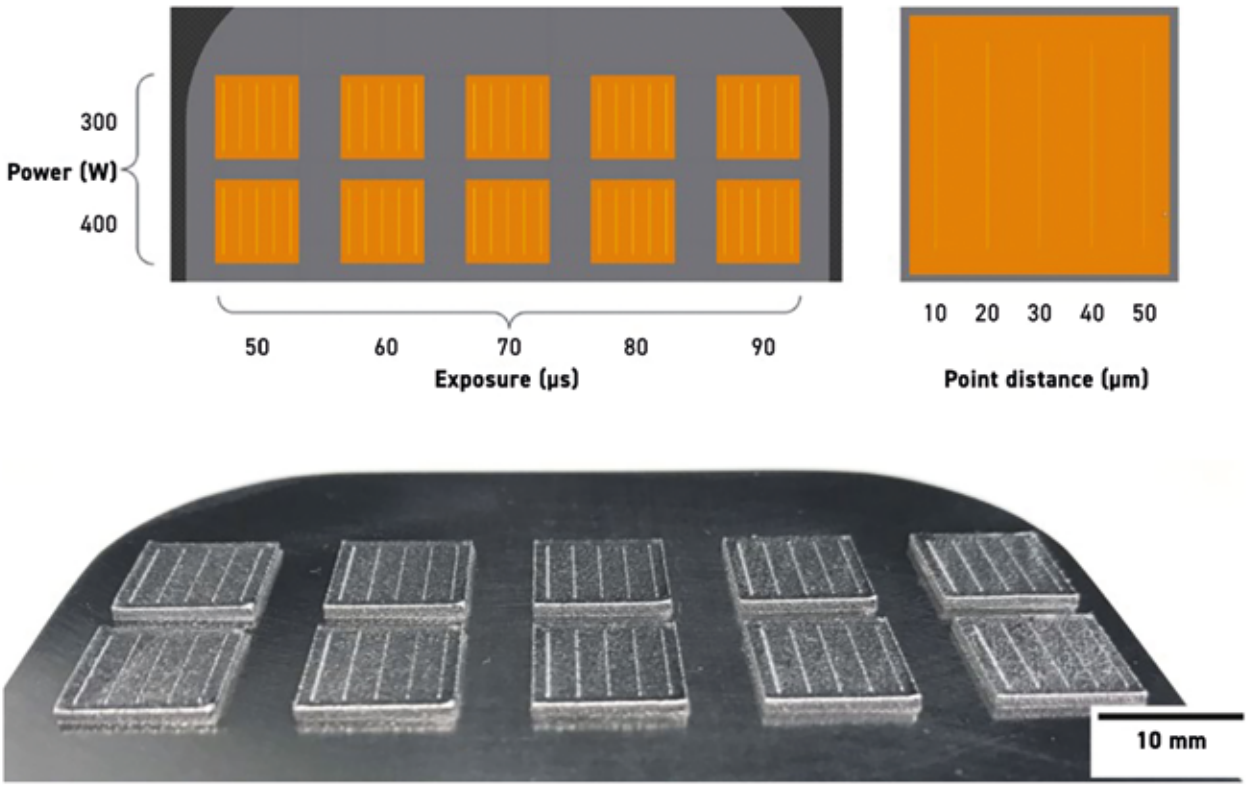

Fig. 7 Single track design of experiments (DOEs) (top) and experiments (bottom) conducted in Renishaw AM 400 machine at 300–400 W with 50–90 µs exposure time and 10–50 µm point distance

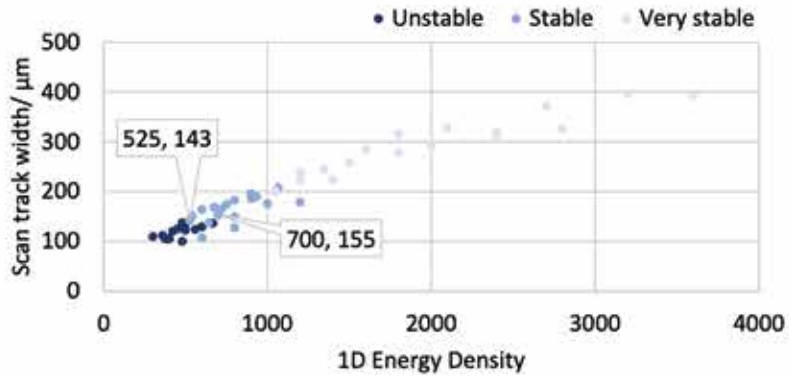

Fig. 8 Process parameter and microstructure stability plot generated by characterising single tracks made from various operating conditions for FS-85

Parameter	Range
Laser power	200 W and 300 W
Exposure time	70 µs
Hatch distance	70 µm to 110 µm in steps of 10 µm
Point distance	30 µm, 40 µm, 50 µm and 70 µm

Table 2 Range of parameters used for design of experiment to determine the additive manufacturability of FS-85 and C-103 alloys

build can be assessed by investigating its density/porosity. It can be seen that, as the laser power (all other parameters remain unchanged) is lowered from 300 to 200 W, defects – or pores – are significantly reduced around the corners, borders and bulk (Fig. 10).

Characterisation of additive manufacturability

Density comparison of C-103 and FS-85

Cubes with density › 99.9 % were obtained by applying optimised processing parameters. A comparison of corners, borders and bulk microstructure has been made and the micrographs for C-103 and FS-85 are shown in Figs. 11 and 12, respectively. It can be seen that both alloys are readily processable through Laser Beam Powder Bed Fusion.

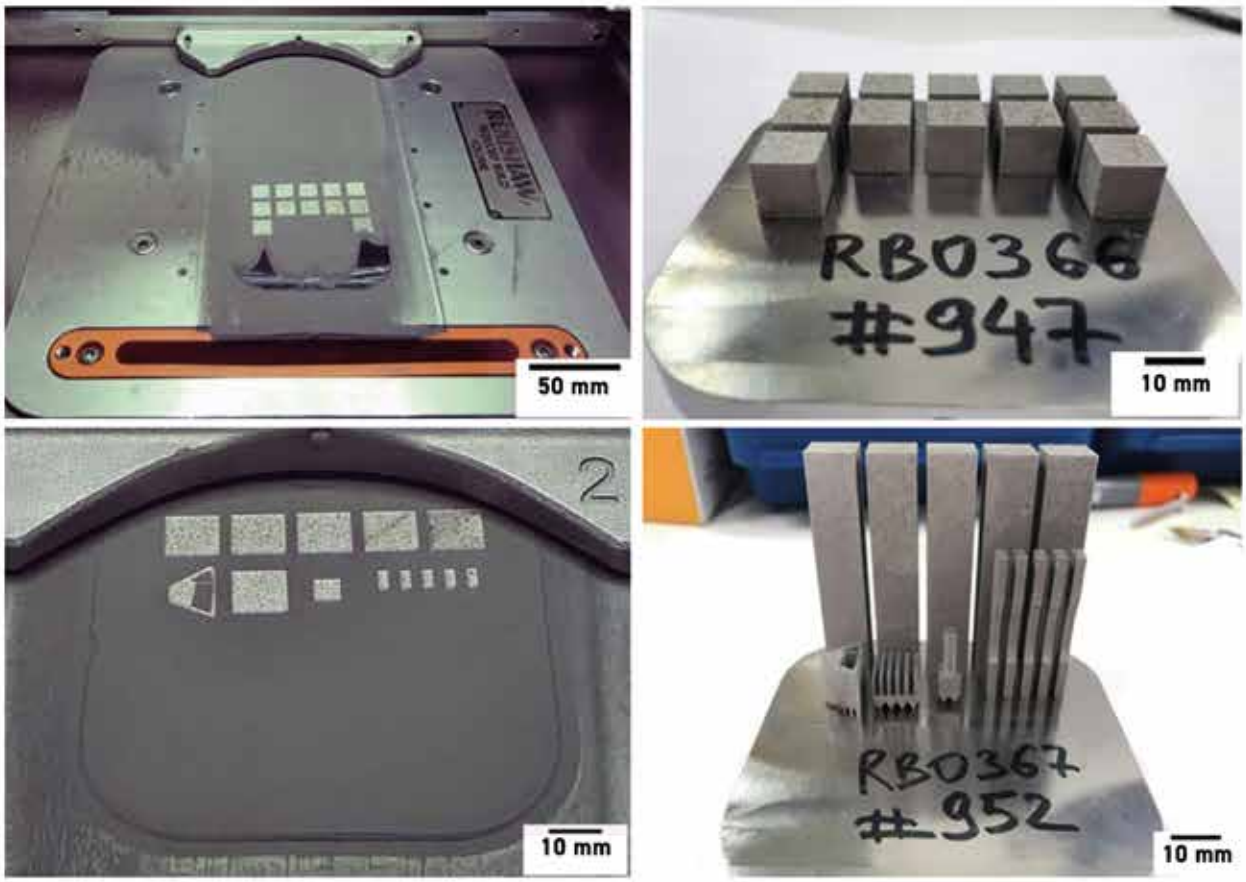

Fig. 9 Cube build of C-103 and FS-85 (top) as a part of the design of experiment strategy. Full test bar build (bottom) with the optimised Additive Manufacturing parameters

Advanced chemical and micro characterisation / EBSD

Additive Manufacturing using PBF-LB has a significant impact on the development of the morphology of the materials used. This can be illustrated for FS-85 by comparing the powder morphology shown in Fig. 5 with that of the material additively manufactured by PBF-LB shown in Fig. 13.

When exposed to the laser beam on the powder bed, the powder melts completely. Moreover, the underlying layers are also melted and, accordingly, each individual layer is remelted several times throughout the process. In the molten layers, the individual atoms are randomly distributed, with maximum disorder; they exhibit maximum entropy. Since the cooling rates for PBF-LB are extremely high at around 10^5 K/s, a thermodynamically favoured partial demixing with the formation of dendrite-like structures observed in the powder particles can no longer take place. The remaining structure, therefore, has a very high entropy and random element distribution.

At the deepest part of the melt pool (i.e., at the solid/liquid boundary), a slight segregation of the alloy may occur. The reason is that the individual alloy components solidify with different rates, causing local segregation. Two such melt pool boundaries are indicated in Fig. 13 in the tungsten map by a dashed line. The melt pool boundaries are likewise visible, though not highlighted, in the Nb, Ta and Zr maps.

To make sure all additively manufactured components fulfilled the composition specification for C-103 and FS-85 standards, advanced chemical analysis such as ICP and LECO were applied. Table 3 shows the oxygen concentration measured using LECO for powders and the final components. This level of quality check is required for the stringent qualification of various classes of components for space applications. In general, a slight increase of oxygen (140–250 ppm) was observed, caused by the PBF-LB processing.

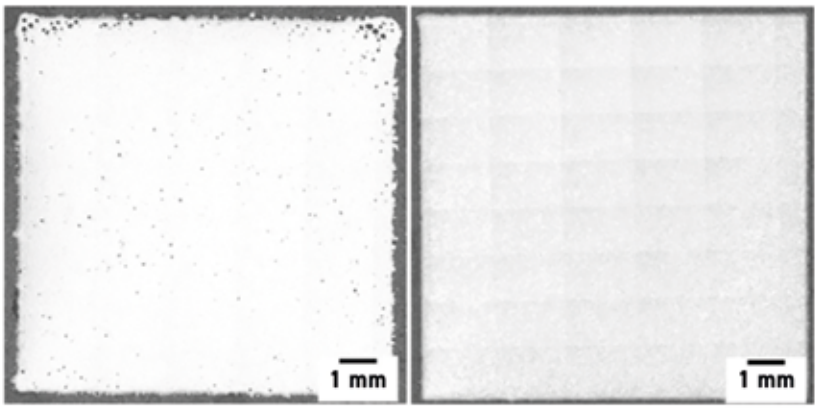

Fig. 10 Optical micrographs of DOE cubes processed at 300 W (left) and 200 W (right), showing significant difference in defect concentration, size and shape

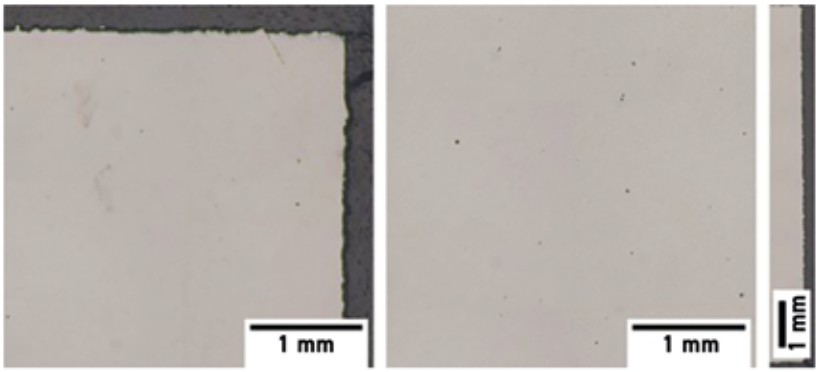

Fig. 11 Optical micrographs of corner (left), bulk (middle) and border (right) showing weak presence of defects/porosities for C-103 cube built with optimised parameters

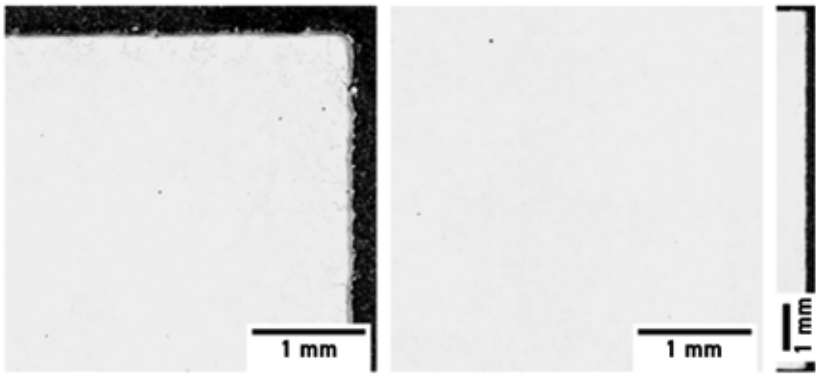

Fig. 12 Optical micrographs of corner (left), bulk (middle) and border (right) showing weak presence of defects/porosities for FS-85 cube built with optimised parameters

Advanced electron back scattered diffraction examination of the AM parts was performed to assess the grain structure in the as-built components. EBSD maps of C-103 and FS-85 (Fig. 14) show predominantly (101) and (111) textures, respectively. This change in texture from cube on the edge to cube on the corner dependence could be attributed to the difference in chemical composition leading to a difference in solidification texture during the Additive Manufacturing of powders using PBF-LB.

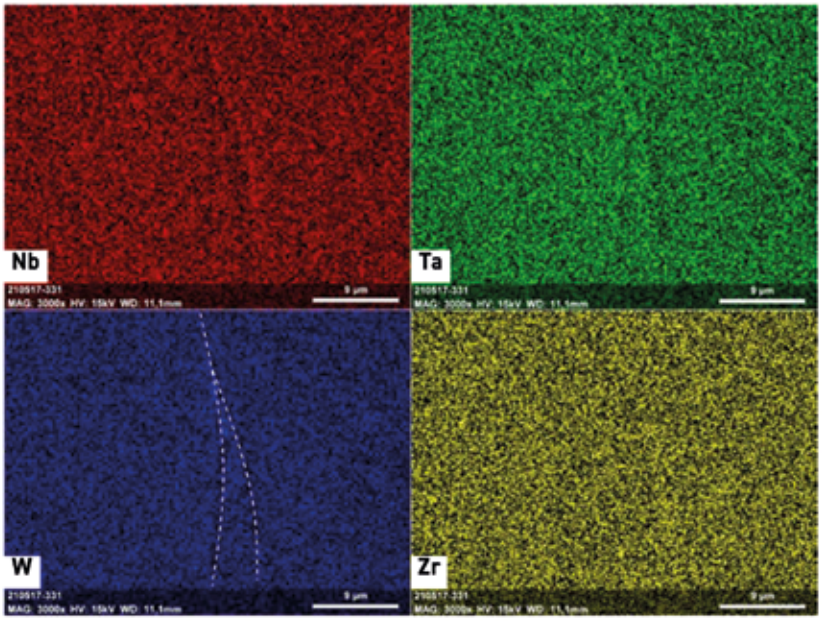

Fig. 13 EDX images of polished cross sections of FS-85 additively manufactured specimens recorded at 3000 x magnification. Build direction was right to left. The dashed line in the W map highlights melt pool boundaries along which a slight demixing occurances

Mechanical performance

The mechanical performance of the additively manufactured FS-85 and C-103 at room temperature was measured using standard ASTM E8 tests. Rectangular blanks of dimension 55 x 10 x 10 mm were machined into cylindrical dumbbell specimens with threads on either end. The samples were tested in tension in a 30 kN Instron tensile testing machine at a strain rate of 0.005 mm/min. Fig. 15 shows the room temperature performance of additively manufactured FS-85 and C-103.

It is found that FS-85 is significantly stronger than C-103. The corresponding ultimate strengths are approximately 750 MPa and 565 MPa, respectively. On the other hand, C-103 exhibits a significantly higher strain-to-failure of ~20–22% compared with ~6–7% in FS-85. Alloyed is currently performing ETMT measurements to investigate the high temperature capabilities of these materials. Experimental details will be published separately [11]. As evident from Fig. 16, an excellent high-temperature performance can be observed for both alloys at elevated temperatures. Either of the alloys produced by PBF-LB is clearly outperforms C-103 in in terms of strength and density compensated strength. In accordance with room temperature investigation, FS-85 is the first choice when searching for new alloys for service in high-temperature environments [11].

Alloy	Source	Process	Oxygen content / ppm	
			Powder	AM coupon
FS-85	Alloyed/Taniobis	PBF-LB	180	398
C-103	Alloyed/Taniobis	PBF-LB	248	423

Table 3 Oxygen content of powders and additively manufactured components measured through LECO for qualification and to understand oxygen pickup during manufacture

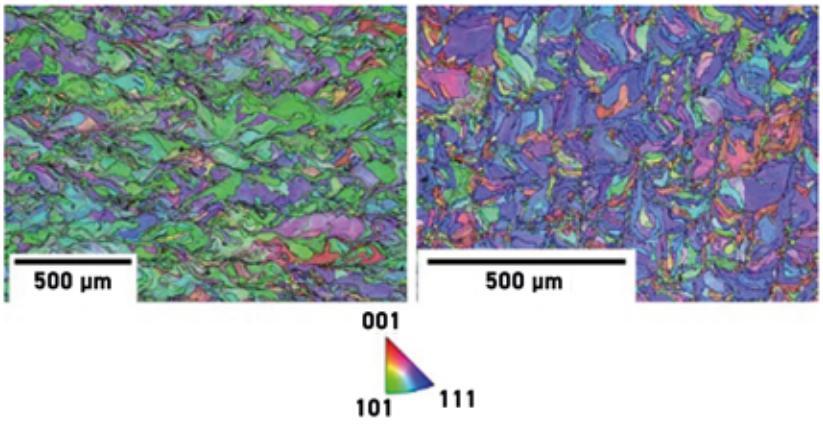

Fig. 14 EBSD of C-103 (left) and FS-85 (right) as-built parts

Outlook for component manufacture

Both these Nb alloys proved to have superior additive manufacturability and mechanical properties comparable to conventionally processed alloys. These alloys, therefore, need to be manufactured into prototype components to prove the validity of these alloys in actual component manufacture for space applications.

Authors

Dr Markus Weinmann
Senior Scientist,
Taniobis GmbH
markus.weinmann@taniobis.com

Dr Shaumik Lenka
Materials Design Engineer,
Alloyed Ltd

Dr David Crudden
Director of Alloy Development,
Alloyed Ltd

Dr André Németh
Director of Group Synergy,
Taniobis GmbH

Dr Melanie Stenzel
Director of Marketing,
Taniobis GmbH

References

[1] V V Satya Prasad, R G Baligidad, Amol A Gokhale, *Niobium and Other High Temperature Refractory Metals for Aerospace Applications in Aerospace Materials and Material Technologies*, Springer Singapore (2017), Eds. N Eswara Prasad, R J H Wanhill

[2] N Philips, M Carl, N J Cunningham, 'New Opportunities in Refractory Alloys,' *Metallurgical and Materials Transactions* 51A (2020) 3301

[3] J Hakl, T Vlasák, J Lapin, 'Creep behaviour and microstructural stability of cast nickel based superalloy IN 792 5A,' *Kovove Mater.* 45 (2007) 177–188

[4] J J Stephens, 'Recent advances in high-temperature niobium alloys,' *JOM* 42 (1990) 22–23

[5] K Chattopadhyay, R Goswami, 'Melting and Superheating of Metals and Alloys,' *Prog. Mater. Sci.* 42 (1997) 287-300

[6] O R Mireles, O Rodriguez, Y Gao, N Philips, 'Additive Manufacture of Refractory Alloy C103 for Propulsion Applications,' as presented at AIAA Propulsion and Energy 2020 Forum, August 24-28, 2020, VIRTUAL EVENT

[7] AMtrinsic® is a registered trademark of Taniobis GmbH

[8] S Pleier, W Goy, B Schaub, M Hohmann, M Mede, R Schumann, 'EIGA-Innovative Production Method for Metal Powder from Reactive and Refractory Alloys,' in Powder metallurgy & particulate materials; proceedings of the international conference on powder metallurgy & particulate materials 2-49-2-55 (2004)

[9] D Huck-Jones, C Langley, 'Beyond particle size: Exploring the influence of particle shape on metal powder performance,' *Metal Additive Manufacturing*, Winter 2017 (Vol. 3 No. 4), pp. 99–103

[10] C Schulze, M Weinmann, C Schweigel, O Kessler, R Bader, Mechanical Properties of a Newly Additive Manufactured Implant Material Based on Ti-42Nb, Materials 11 (2018) 124

[11] S Lenka, *et al.* In preparation for publication

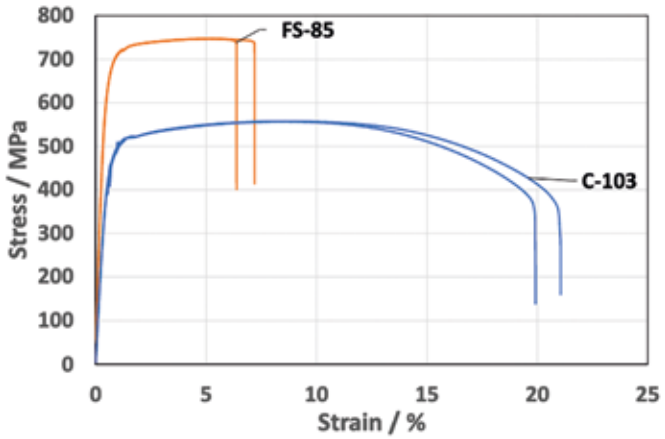

Fig. 15 Mechanical properties of C-103 and FS-85 alloys at room temperature processed by PBF-LB

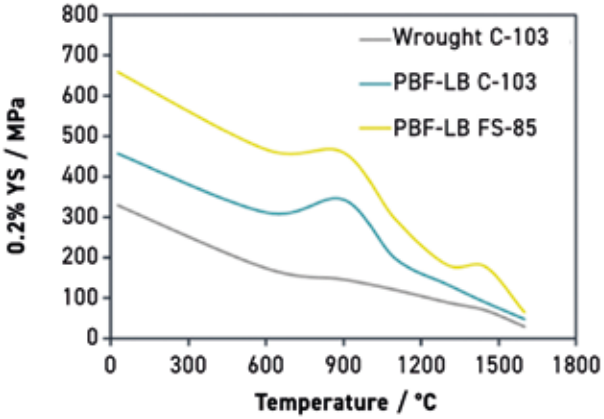

Fig. 16 High-temperature tensile tests (ETMT) of yield strength C-103 and FS-85 processed by PBF-LB

For questions to **AMtrinsic®** powders contact:

TANIOBIS GmbH
Im Schleeke 78 - 91
38642 Goslar
Germany
amtrinsic@taniobis.com